Biochemistry and Biophysics Reports 20 (2019) 100670

Contents lists available at ScienceDirect

Biochemistry and Biophysics Reports

journal homepage: www.elsevier.com/locate/bbrep

# Characterization of human serum albumin's interactions with safranal and crocin using multi-spectroscopic and molecular docking techniques

Alaa A. Salem[a,*], Mohamed Lotfy[b], Amr Amin[b], Mohammad A. Ghattas[c]

[a] Department of Chemistry, College of Science, United Arab Emirates University, Al Ain, P.O. Box 15551, United Arab Emirates
[b] Department of Biology, College of Science, United Arab Emirates University, Al Ain, P.O. Box 1551, United Arab Emirates
[c] College of Pharmacy, Al Ain University of Science and Technology, P.O. Box 112612, Abu Dhabi, United Arab Emirates

ARTICLE INFO

*Keywords:*
Human serum albumin. safranal
Crocin
UV–Vis
Fluorescence quenching
Circular dichroism
Molecular docking

ABSTRACT

Interaction mechanisms of human serum albumin (HSA) with safranal and crocin were studied using UV–Vis absorption, fluorescence quenching and circular dichroism (CD) spectroscopies as well as molecular docking techniques. Changes in absorbance and fluorescence of HSA upon interactions with both compounds were attributed to their binding to amino acid chromophores located in subdomains IIA and IIIA. Fluorescence secondary inner filter effect was excluded using 278 nm and 340 nm as the wavelengths of HSA's excitation and fluorescence while safranal and crocin absorbed at 320 nm and 445 nm, respectively. Stern-Volmer model revealed a static quenching mechanism involve the formation of non-fluorescent ground state complexes. Stern-Volmer, Hill, Benesi-Hilbrand and Scatchard models gave apparent binding constants ranged in $4.25 \times 10^3$ - $2.15 \times 10^5$ for safranal and $7.67 \times 10^3$ - $4.23 \times 10^5$ L mol$^{-1}$ for crocin. CD measurements indicated that 13 folds of safranal and crocin unfolded the α-helix structure of HSA by 7.47–21.20%. In-silico molecular docking revealed selective exothermic binding of safranal on eight binding sites with binding energies ranged in −3.969 to −6.6.913 kcal/mol. Crocin exothermally bound to a new large pocket located on subdomain IIA (sudlow 1) with binding energy of −12.922 kcal/mol.

These results confirmed the formation of HSA stable complexes with safranal and crocin and contributed to our understanding for their binding characteristics (affinities, sites, modes, forces … etc.) and structural changes upon interactions. They also proved that HSA can solubilize and transport both compounds in blood to target tissues. The results are of high importance in determining the pharmacological properties of the two phytochemical compounds and for their future developments as anticancer, antispasmodic, antidepressant or aphrodisiac therapeutic agents.

## 1. Introduction

Saffron, the food flavoring and coloring substance, has a long history of use as a traditional medicine. It is derived from the natural *Crocus sativus* flowers' dried stigma (family: iridaceae) [1,2]. Saffron has a plethora of biological activities that include antispasmodic, antidepressant, aphrodisiac, respiratory decongestant and a remedy against scarlet fever, asthma, and smallpox [3,4]. The major bioactive constituents in saffron include safranal (1.5%), picrocrocin (6.0%), and the yellow colored compound crocin (86.5%) [5].

Safranal (2,6,6-trimethyl-1,3-cyclohexadiene-1-carboxaldehyde) is a volatile monoterpene aldehyde produced by acidic hydrolysis of picrocrocin [6] (Fig. 1). Safranal represents around 70% of saffron's aroma and is a major component of saffron's oil [7]. Safranal has proven antioxidant [8], genoprotective [9], bronchodilatory [10], cytotoxic [11], antitussive [12], anticonvulsant [13], antinociceptive [14], neuroprotective [15], antiabsence [16], antidepressant [17], hypotensive [18], anxiolytic and hypnotic pharmacological effects [19].

Several cellular proteins include cytochrome b-c1 complex sub-unit 1, trifunctional enzyme sub-unit beta, ATP synthase sub-units (α and β) in liver cells and Beta-actin-like protein 2 in kidney, heart and brain cells were identified as molecular targets for safranal. It was also reported that safranal acts as a protective agent against DNA damage induced by methyl methane sulfonate in mice organs [9,20].

Crocin is the glycosylic ester of crocetin. It is hydrolyzed during intestinal absorption to crocetin (Fig. 1). Crocin's antioxidant, anti-inflammatory and anticancer effects have been documented [4]. Protection of cells against oxidative damage by crocin was attributed to its biological antioxidant effect that quenches the damaging singlet oxygen and free radicals formed during lipid's oxidation [21]. Crocin has also

* Corresponding author.
*E-mail address:* Asalem@uaeu.ac.ae (A.A. Salem).

https://doi.org/10.1016/j.bbrep.2019.100670
Received 4 May 2019; Received in revised form 16 July 2019; Accepted 17 July 2019
Available online 12 September 2019

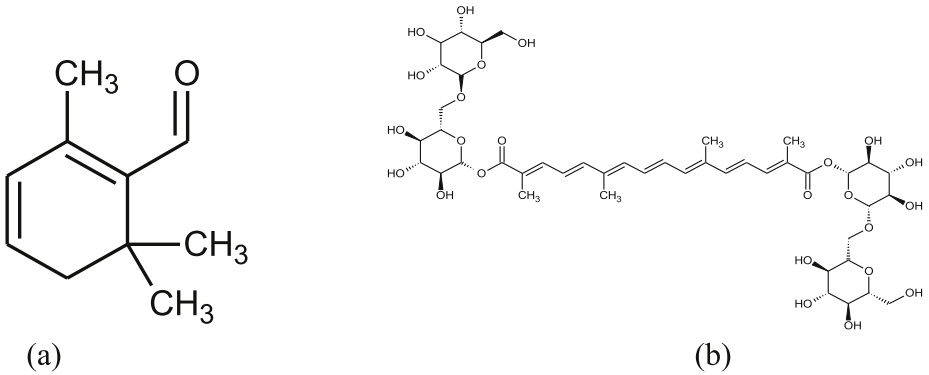


**Fig. 1.** Structural formulas of safranal (a) and crocin (b).

shown to reduce lipidemia in rats and affect memory and learning in animal models [22,23]. Crocetin has shown to inhibit syntheses of DNA and RNA in isolated nuclei and to suppress the activity of purified RNA polymerase-II [24].

Both crocin and crocetin were shown to inhibit the proliferation of HL-60 leukemic cells and differentiate them in a comparable pattern to trans-retinoic acid [25]. Crocins and dimethyl-crocetin were found non-mutagenic, nontoxic and anticarcinogenic [26]. The effects of crocin and crocetin on histone H1 structure and H1–DNA interaction were also investigated [27]. Complexation of safranal, crocetin and dimethyl-crocetin with DNA resulted in partial transitions of DNA from the B to A forms. Stability order of adducts formed is dimethyl-crocetin > crocetin > safranal [28].

On the other hand, human serum - albumin as the most abundant protein represents - about half of human blood serum (~35–55 g/L) and has a half-life of approximately 20 days. HSA is produced in liver as monomeric globular soluble protein with many physiological and pharmacological functions. It transports endogenous and exogenous compounds such as drugs, fatty acids, vitamins, bilirubin, metabolites and amino acids in blood [29]. The extraordinary ability of HSA to reversibly bind various drugs in plasma enables it to control their distribution patterns to different target tissues during plasma circulation [30], pharmacokinetics and osmotic pressures [31,32]. However, strong binding has been correlated with increase in release time and subsequent diminish in the therapeutic values of drugs whereas weak binding has been correlated with poor absorption of drugs and delay in their delivery rates and reaching action sites. The moderate binding capacity of HSA has made it the model protein of choice for studying the physiochemical and biophysical behaviors of drugs' transports to target tissues [33,34].

Human serum albumin consists of a single polypeptide chain contains 585 amino acid residues in three structurally similar domains (I, II and III) forming two subunits connected with 17 disulfide bonds [35]. The polypeptide chain forms a heart-shaped structure with approximate dimensions of 80 × 80 × 80 $Å^3$ and a thickness of 30 Å. About 67% of HSA is α-helix and no β-sheets in the three structurally homologous domains (I, II and III) [29,36]. Each domain contains 10 helices with helices 1–6 form the respective sub-domains A and helices 7–10 comprise sub-domains B. Aromatic and heterocyclic ligands bind within two hydrophobic pockets in the sub-domains IIA and IIIA. Seven binding sites are localized for fatty acids in the sub-domains IB, IIIA, IIIB and sub-domain interfaces. The two major binding sites located in sub-domains II and III are named as sudlow 1 and sudlow 2. Several other binding sites have been identified for HSA (Fig. 2) [37].

These multiple binding sites underlie the exceptional ability of HSA to interact with many drugs, regulate their intercellular fluxes, pharmacokinetic and pharmacodynamics behaviors [38].

Several crystal structures of HSA complexed to different drugs are cited in the RCSB-PDB. Examples include HSA complexed with warfarin (2BXD), diazepam (2BXF), azapropazone (2BX8), ibuprofen (2BXG),

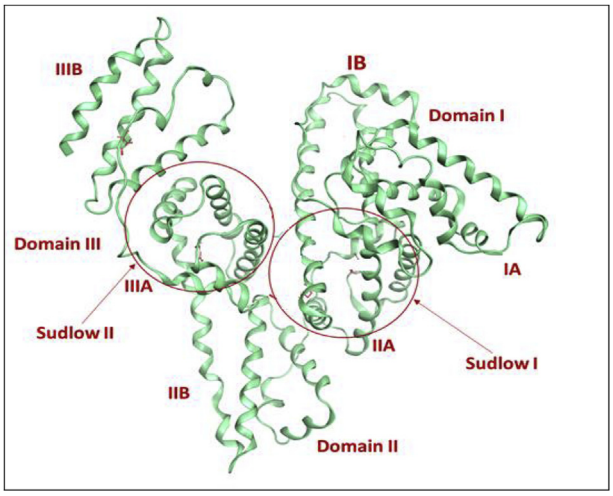


**Fig. 2.** Representation of domains, subdomains and sudlow binding sites on human serum albumin.

indomethacin (2BXK), iodipamide (2BXN), myristate-1 (2BXQ) and myristate-2 (2BXP).

Due to the limited toxicity of safranal and crocin and their biological activity as antioxidant, anti-inflammatory, anticancer, antigenotoxic and antiaging, study of their interaction mechanisms with human serum albumin is crucial in determining their pharmacological properties. This work aimed to study such interaction mechanisms at the physiological pH using various spectroscopic techniques along with molecular docking. UV–Vis molecular absorption, fluorescence quenching and circular dichroism were used to monitor structural changes in HSA upon binding with both compounds and evaluate their binding affinity and stoichiometry of complexes formed. The inner filter effects were excluded using excitation wavelength of 278 nm and fluorescence wavelength of 340 nm for HSA while safranal and crocin absorbed strongly at 320 and 445 nm, respectively. Molecular docking of both compounds on HSA crystal structure was done using the Glide software tool.

The results obtained of this work gave insights on the role of HSA in distributing safranal and crocin to target tissues and in determining their pharmacological properties. The results are crucial for the development of safarnal or crocin based therapeutics drugs. Though binding of safranal with HSA has been reported, previous report suffered from errors caused by inner filter effects and ambiguity in determining the exact binding modes and sites [39]. On contrary, study of interaction of crocin with HSA has never been reported up-to-date.

## 2. Materials and methods

### 2.1. Materials

The highest purity available materials were used. Lyophilized powder of human serum albumin ($66.5 \times 10^3$ Da), safranal (150.21 Da), crocin (976.97 Da), dimethyl sulfoxide (DMSO) and phosphate buffer saline (PB) tablets were purchased from Sigma-Aldrich (St. Louis, MO, USA). Distilled deionized water was used throughout.

### 2.2. Apparatus

All UV–Vis absorption measurements were carried out using a LAMBDA-25 UV–Vis spectrophotometer (PerkinElmer, USA) supported with 1.0 cm matched quartz cells.

Fluorescence measurements were carried out using Cary Eclipse model-3 spectrofluorometer equipped with a high intensity Xenon flash lamp and 1.0 cm path length quartz cell (Varian, Austria).

Circular dichroism measurements were made using a Jasco-J-815 spectrometer (Jasco, USA).

All pH measurements were made using Orion-401-Plus pH meter supported with Orion glass electrode (USA).

### 2.3. Standard solutions

A 0.01 M phosphate buffer (PB) solution (pH 7.4) was prepared by dissolving one PBS tablet in 200.0 ml of deionized water. The pH of the solutions was adjusted using the glass electrode.

A $10^{-3}$ M stock solution of safranal was prepared by dissolving 7.51 mg into 2.5 ml DMSO. The solution was made up to 50.0 ml using PB solution pH 7.4.

A $10^{-3}$ M stock solution of the water soluble crocin was prepared by dissolving 0.098 mg of crocin into 100.0 ml PB solution.

A stock HSA solution ($7.50 \times 10^{-6}$ M) was prepared by dissolving 50.0 mg of HSA into 100.0 ml PB solution, pH 7.4. The solution was kept refrigerated and protected from light.

Solutions having lower concentrations were prepared by appropriate dilutions of the above stock solutions in PB solution, pH 7.4.

### 2.4. Procedures

Interactions of HSA with safranal and crocin were studied using UV–Vis absorption, fluorescence and circular dichroism spectrophotometric techniques. Interaction parameters including binding constants, binding stoichiometry and binding modes were evaluated.

#### 2.4.1. UV–vis absorption titration

UV–Vis titrations were carried out by adding successive portions of safranal or crocin ($1 \times 10^{-4}$ M) to HSA ($7.5 \times 10^{-6}$ M) in PB solution, pH 7.4. Titrations were reversed by adding successive amounts of HSA ($7.5 \times 10^{-6}$ M) to ($1 \times 10^{-4}$ M) safranal or crocin in PB solution, pH 7.4. After each addition, solutions were shacked, incubated for 1.0 min at room temperature and scanned in the range 200–700 nm. Titrations were stopped at saturation when no change in absorbance was observed. Absorbance readings at $\lambda_{max}$ were corrected for dilution effect and plotted versus volume added of the titrants. PB solution was used as a blank in all measurements.

#### 2.4.2. Fluorescence titration

HSA gave a fluorescence band at 340 nm when excited at 278 nm. Therefore, interactions of HSA with safranal and crocin were followed fluorometrically at 340 nm. Successive μl portions of safranal or crocin ($1.0 \times 10^{-3}$ M) were added to 2.0 ml HSA ($7.5 \times 10^{-6}$ M) in PB solution, pH 7.4. After each addition, solutions were shacked, incubated for 1.0 min and scanned for its fluorescence in the range 280–600 nm. A 2.5 nm excitation and emission slit widths was applied in all measurements. Titrations were stopped when no changes in fluorescence intensity were observed.

On the other hand, safranal gave fluorescence emissions at 385 nm when excited at 320 nm. Therefore, interactions of HSA with safranal was followed by reversing the above experiment and following safranal' emission at 385 nm. Successive amounts of HSA ($7.5 \times 10^{-6}$ M) were added to safranal ($1 \times 10^{-4}$ M) in PB solution, pH 7.4. After each addition, solutions were shacked, incubated for 1.0 min and scanned for its fluorescence in the range 280–600 nm using excitation and emission slit widths of 2.5 nm. Titrations were stopped when no or slight changes in fluorescence intensity were observed.

#### 2.4.3. Circular dichroism

Circular dichroism was used to confirm results obtained by UV–Vis and fluorescence spectroscopies. Interactions of safranal and crocin with HSA were followed by adding 20.0 μl successive portions of safranal or crocin ($1.0 \times 10^{-3}$ M) to 2.0 mL HSA ($7.5 \times 10^{-6}$ M) in PB solution, pH 7.4. After each addition, solution was shacked well, incubated for 2.0 min at room temperature and scanned for its CD in the range 200–300 nm. A scan speed of 50.0 nm/min and a bandwidth of 1.0 nm were applied. Spectra were averaged over at least three scans. All CD spectra were baseline corrected against blank solutions.

#### 2.4.4. Binding affinity

*2.4.4.1. Fluorescence quenching.* The fluorescence quenching' rate constants for HSA upon additions of safranal or crocin were determined using Stern–Volmer equation [40].

$$F_0/F = 1 + k_q\tau_0[Q] = 1 + K_{SV}[Q] \quad (1)$$

where F and $F_0$ are the fluorescence intensities in presence of different safranal or crocin concentrations, kq is the quenching rate constant, $K_{SV}$ is the Stern–Volmer constant, $\tau_0$ is the fluorescence lifetime of HSA and [Q] is the concentration of safranal or crocin. A plots of $F_0/F$ versus [Q] gives a linear plot whose slop equals $K_{SV}$.

Fluorescence quenching of HSA's was also used to estimate binding affinities of HSA towards safranal and crocin using the Stern-Volmer equation [41].

$$F_0 / F = 1 + (1/[Q] \text{ x } 1/f\,K) + (1/f) \quad (2)$$

where $F_0$ and F are the fluorescence intensities of HSA in absence and presence of quencher, respectively. f is the fractional maximum fluorescence intensity of protein summed up and K is a constant. A graph of $F_0/F$ versus the reciprocal of quencher's concentration (1/[Q]) yields a linear plot whose slop equals $(fK)^{-1}$ and ordinate's intercept equals $f^{-1}$. The association constant K is obtained by dividing $f^{-1}$ over $(fK)^{-1}$.

Fluorescence quenching were also used to estimate binding affinities and number of binding sites of HSA towards safranal and crocin using Hill plot model (equation (3)).

$$\text{Log}\frac{F0 - F}{F} = \text{Log } k + n \text{ Log}[Q] \quad (3)$$

where $F_0$ and F are the fluorescence intensities in the absence and presence of drug, K is the binding constant with HSA, and n is the number of binding sites. Changes in fluorescence intensity of HSA upon additions of safranal or crocin were recorded and Hill plots of log $(F_0–F)/F$ versus log Q was constructed.

*2.4.4.2. Absorbance changes.* Changes in UV–Vis absorption spectra of HSA upon additions of different increments of safranal or crocin were used for determining their binding constants. Absorbance's changes at 280 nm indicate alterations in the close proximities of the aromatic amino acid residues [42,43].

According to Benesi and Hildebrand [44], the apparent association constant $K_{app}$ can be calculated as follows:

$$A_{obs} = (1- \alpha)\ C_o\ \varepsilon_{HSA}\ l + \alpha\ C_o\ \varepsilon_c\ l \quad (4)$$

where $A_{obs}$ is the absorbance of the HSA solution at different drug's concentrations at 279 nm, α is the degree of association between HSA and drug molecules, $\varepsilon_{HSA}$ and $\varepsilon_c$ are the molar absorptivity at 279 nm for HSA and the complex, respectively, $C_o$ is the initial concentration of HSA and l is the optical path length.

Replacing $C_o\ \varepsilon_c\ l$ by A, equation (5) can be expressed as

$$A_{obs} = (1- \alpha)\ A_o + \alpha\ A_c \quad (5)$$

Where $A_o$ and $A_c$ are the absorbance of HSA and the complex at 279 nm, respectively with the concentration of $C_o$.

At relatively high drug concentration, α can be equated to ($K_{app}$ [drug])/(1 + $K_{app}$ [drug]) where [drug] is the concentration of drug in mol/L. Thus Eq. (6) now becomes.

$$\frac{1}{A_{obs}-Ao} = \frac{1}{Ac - Ao} + \frac{1}{K_{app}\,(Ac - A_0)[drug]} \quad (6)$$

A graph of $1/(A_{obs} - A_o)$ versus 1/[ drug], yield a linear plot with a slope equals to $1/K_{app}\ (A_c - A_o)$ and an intercept equals to $1/(A_c - A_0)$. Thus $K_{app}$ can be calculated by dividing the intercept with slop.

On the other hand, Scatchard model was also used to estimate the binding constants number of binding sites based on changes in absorption spectra of safranal and crocin upon additions of HSA by applying equation (7).

$$r/C_f = nK - Kr \quad (7)$$

where r is the number of moles of safranal or crocin bound to 1 mol of HSA ($C_b/C_{HSA}$), n is the number of equivalent binding sites per HSA molecule and K is the binding affinity. The free and bound concentrations of safranal or crocin ($C_f$, $C_b$) were calculated using $C_f = C_{total}$ (1 - α) and $C_b = C_{total}$ - $C_f$, respectively. $C_{total}$ is the total concentration of safranal or crocin at zero addition of HSA and α is the fraction of bound safranal or crocin calculated as $\alpha = (A_f - A)/(A_f - A_b)$. $A_f$, A and $A_b$ are the UV–Vis absorbance at zero addition, after each addition and at saturation, respectively. Scatchard plot gives a slope equals the binding constant K and an intercept equals nK [45].

### 2.5. Molecular docking of safranal and crocin into HSA binding sites

Preparation of HSA for docking was done by downloading the crystal structures of HSA complexed with warfarin, diazepam, azapropazone, ibuprofen, indomethacin, iodipamide, myristate and other drugs from the protein data bank. The co-crystallized ligand and water molecules were removed from the protein structure using the molecular operating environment (MOE) software preparation wizard [46]. The crystal structures were subsequently checked for missing atoms, residues or loops and all required corrections were performed. The prepared structures were processed by the Maestro protein preparation module to set up partial charges on each atom and protonation states on each ionizable group [47]. The co-crystallized ligand was used to define the binding site then a grid box was created using the Receptor Grid Generation in Glide [48].

Safranal and crocin were prepared using the build panel in MOE and energy minimized via the Maestro program and the OPLS force field [47,49].

Molecular docking was done by docking the prepared safranal and crocin into the previously identified binding sites using the Glide docking tool applying extra-precision (XP) algorithm for conformational sampling [48,50]. The resultant poses were given scores via the Glide-XP scoring function which includes terms for van der Waals, hydrogen bonding, electrostatic interactions, de-solvation penalty and penalty for intra-ligand contact [50].

## 3. Results and discussion

Human serum albumin is a major circulatory protein with binding affinity towards many endogenous and exogenous compounds. Binding of HSA to drugs, minimizes their free plasma concentration, increases their lifetime, improves their distribution, enhances their efficacy and alters HSA's conformational structure. Two major binding sites are reported on HSA; a large hydrophobic cavity in the subdomain IIA (sudlow 1) with one tryptophan residue (Trip 214) and a small hydrophilic cavity in the subdomain IIIA (sudlow 2) [41]. Interaction modes of HSA to drugs are dependent on their molecular structures as well as their hydrophobic and hydrophilic natures.

In the following sections, we will gain insights on the interaction mechanisms of safranal and crocin with HSA applying UV–Vis absorption, fluorescence and circular dichroism spectroscopies in conjunction with molecular docking. Characterization of these interactions is a crucial step towards any future development of safranal and crocin based therapeutic agents.

### 3.1. UV–vis absorption titrations

Figs. 3 and 4 show the UV–Vis spectra of HSA, safranal and crocin. HSA exhibited an absorption band at 278 nm that can be attributed to π-π* electronic transition in the aromatic π system of tyrosine, tryptophan and cytosine chromophores. Safranal exhibited a strong absorption band at 320 nm caused by n-π* electronic transition [21,39]. Crocin showed three absorption bands characteristics of the 13-cis glycosidic carotenoid structure. The first one at 260 nm corresponds to the glucosyl ester bond of crocin. The second is a medium intensity band at 325 nm attributed mainly to the presence of cis double bonds in the polyene conjugated system of crocin. The third band between 400 and 500 nm with two maxima centered at $\lambda_{max}$ = 445 nm, is characteristic of all trans-carotenoids [51]. The 325 nm broad absorption band can be attributed to π-π* transition while the strong 445 nm band might be caused by charge transfer transition.

Fig. 3a also shows the effect of successive additions of HSA ($7.5 \times 10^{-6}$ M) to safranal ($1 \times 10^{-4}$ M). A steady decrease in the intensity of the 320 nm band (hypochromic effect) associated with slight red shifting were observed. At higher HSA's concentrations, an isoesbestic point is formed at ~285 nm. In Fig. 3b, the titration was reversed by adding increments of safranal ($1 \times 10^{-4}$ M) to HSA ($7.5 \times 10^{-6}$ M). This resulted in increases in the absorption intensity of the safranal band at 320 and the intensity of the HSA band at 278 nm associated with slight red shifting.

On the other hand, titration of crocin with HSA is shown in Fig. 4a. Successive additions of HSA ($7.5 \times 10^{-6}$ M) to crocin ($1 \times 10^{-4}$ M) resulted in steady decreases in the intensity of the three cis-crocin bands at 260, 325 and 445 nm (hypochromic effect). Reversing the titration by adding crocin ($1 \times 10^{-4}$ M) to HSA ($7.5 \times 10^{-6}$ M) is shown in Fig. 4b. Additions of crocin increments resulted in increasing the absorption intensity of the HSA band at 278 nm and the crocin's bands at 260, 325 and 445 nm with no red shifting.

The decrease in the intensities of safranal and crocin band maxima upon additions of HSA can be attributed to their penetrations inside the protein molecule (Figs. 3a and 4a). The presence of excess safranal or crocin in solution favors the formation of labile HSA-safranal or HSA-crocin complex molecules. This subsequently limits the mobility and amount of energy gained by both molecules, causing decreases in their absorption capabilities.

On the other hand, the presence of excess HSA during its titration with safranal or crocin can possibly favors external binding on the protein surface (Figs. 3b and 4b). Since interactions of safranal or crocin ligands on the protein's surface do not limit their motilities around HSA molecule or exposure to light, they increase the absorption intensities [22].

These observed spectral changes upon titrations suggest an

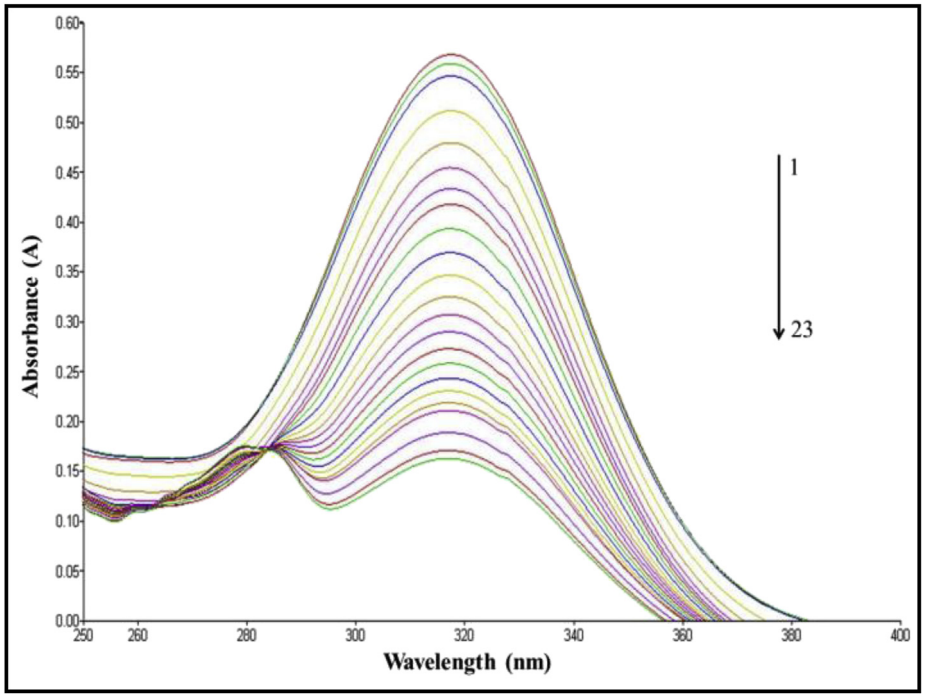


**Fig. 3a.** UV–Vis titration of safranal ($1 \times 10^{-4}$ M) with μl increments of HSA ($7.5 \times 10^{-6}$ M).

interaction process resulted in binding safranal or crocin to HSA and the formation of safranal-HSA or crocin-HSA complex structures.

### 3.2. Fluorescence titrations

In our measurements, safranal gave a fluorescence emission band at 385 nm when excited at 320 nm attributed to the π*-π transition while crocin did not fluoresce. On the other hand, eexcitation of HSA at 278 nm induced a strong fluorescence emission band at 340 nm. This fluorescence emission is attributed to the one tryptophan residue (Trp-214) and the 18 tyrosine residues located in the hydrophobic cavity of subdomain IIA. Exposure of HSA to UV light at 278 nm excites tyrosine residues followed by subsequent energy transfer from the excited tyrosine to tryptophan residue. Relaxation of excited tryptophan results in fluorescence emission band at ~340 nm [52]. Thus, fluorescence emission of HSA caused by excitation at 278 nm is a contribution from both tryptophan and tyrosine. However, the contribution of tyrosine in fluorescence emission can be negated when HSA is excited at 295 nm [53].

In our work, we choose to excite HSA at 278 nm to avoid errors caused by the inner filter effects. Since safranal absorbs maximally at $\lambda_{max}$ = 320 nm and HSA fluoresce maximally at $\lambda_{max}$ = 340 nm, this makes $\Delta_{\lambda}$ of 20 nm which has considered enough to avoid secondary inner filter effect caused by absorption of emitted fluorescence. The

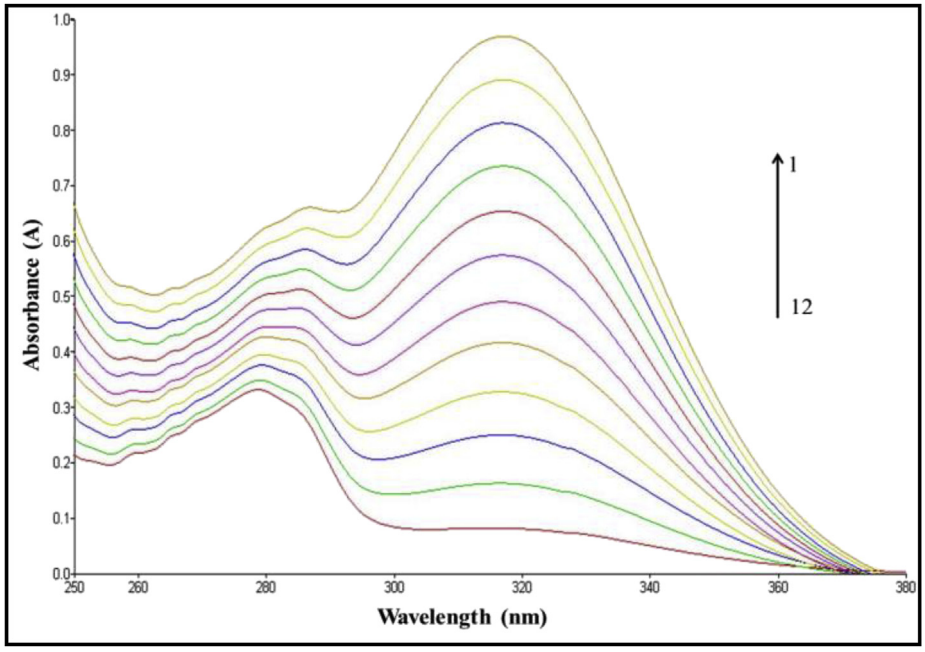


**Fig. 3b.** UV–Vis titration of HSA ($7.5 \times 10^{-6}$ M) with μl increments of safranal ($1 \times 10^{-4}$ M).

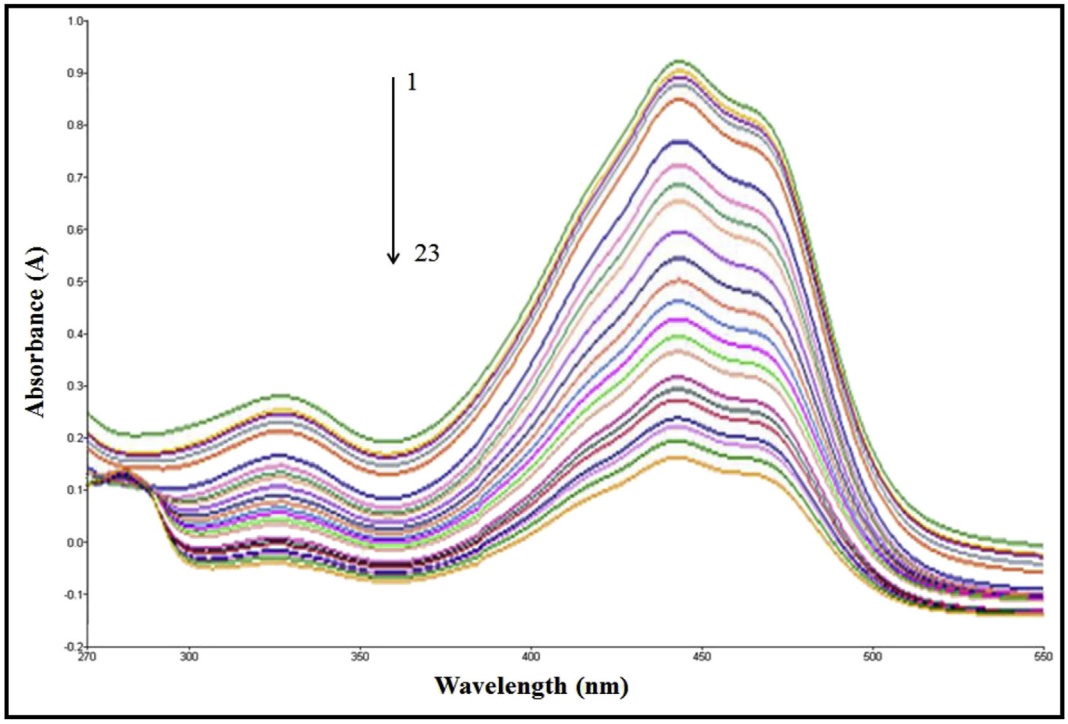


**Fig. 4a.** UV–Vis titration of crocin ($1 \times 10^{-4}$ M) with 0.5 μl increments HSA ($7.5 \times 10^{-6}$ M).

primary inner filter effect in our measurement has been excluded by working with diluted safranal solution [53].

Fig. 5 shows the fluorescence titrations of HSA with safranal and crocin. Successive additions of HSA ($7.5 \times 10^{-6}$ M) to safranal ($1 \times 10^{-4}$ M) decreased the intensity of safranal's fluorescence emission at 385 nm associated with slight shifting to longer wavelength (Fig. 5a).

The reversed titration in which successive increments of safranal ($1 \times 10^{-3}$ M) were added to HSA ($7.5 \times 10^{-6}$ M) is shown in Fig. 5b. A sharp decrease in the fluorescence intensity of HSA at 340 nm reaching 90% at molar ratio of $2.5 \times 10^{-3}$ ([Safranal]/[HSA]) was observed. Quenching of HSA' fluorescence was associated with red-shifting of the fluorescence $\lambda_{max}$ from 340 nm to 356 nm.

In Fig. 5c, additions of crocin ($1 \times 10^{-3}$ M) to HSA ($7.5 \times 10^{-6}$ M) quenched the fluorescence at 340 nm by 60% at molar ratio of $6.6 \times 10^{-4}$ ([Crocin]/[HSA]). This fluorescence quenching was also

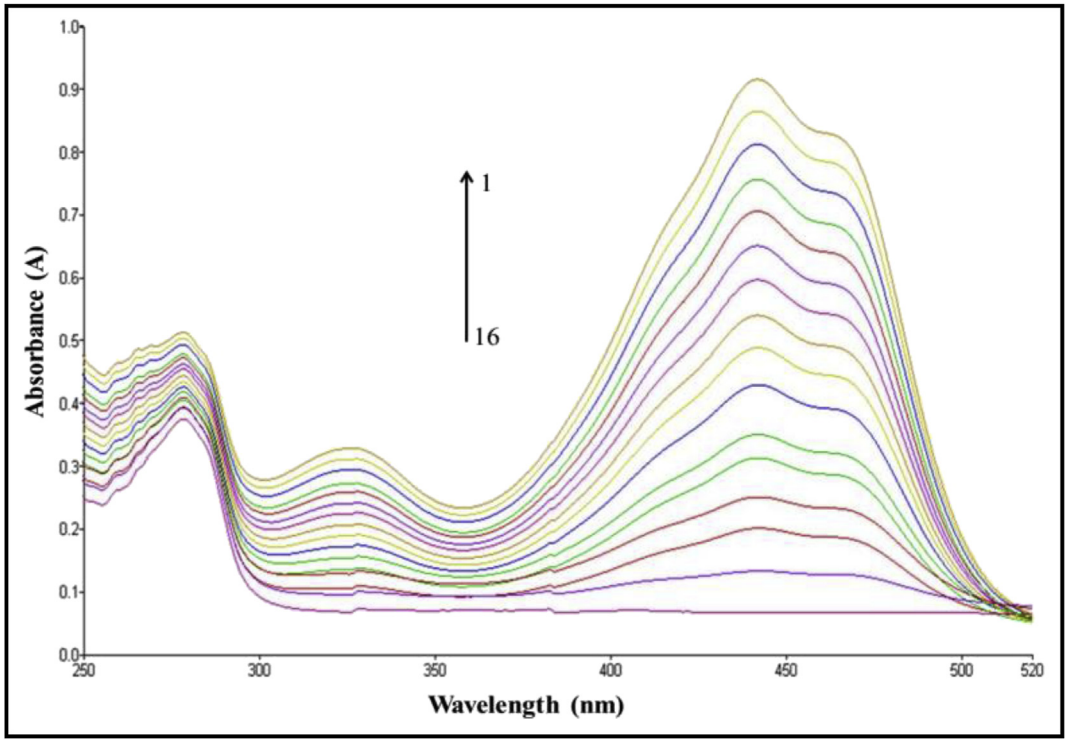


**Fig. 4b.** UV–Vis titration of HSA ($7.5 \times 10^{-6}$ M) with 5.0 μl increments of crocin ($1 \times 10^{-4}$ M).

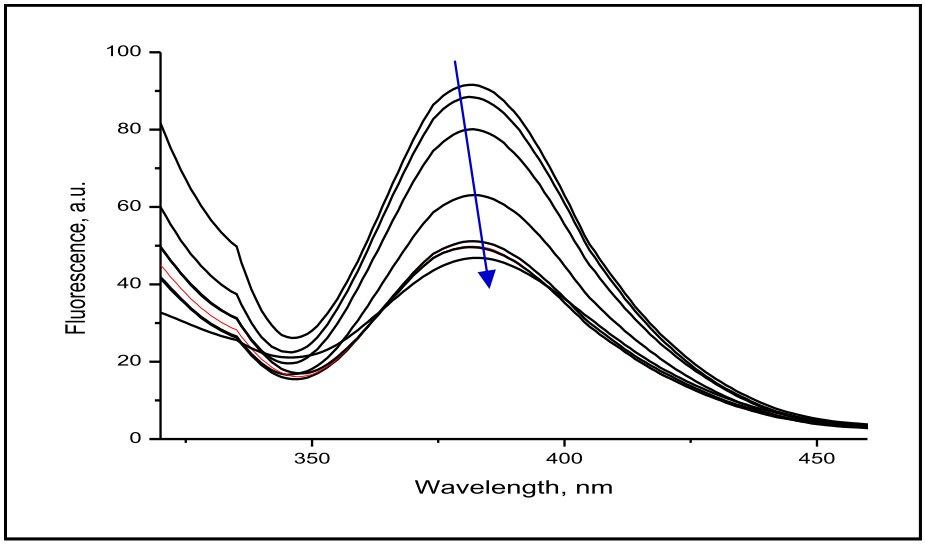


**Fig. 5a.** Fluorescence titration of safranal ($1 \times 10^{-4}$ M) with 0.2 μl increments of HSA ($7.5 \times 10^{-6}$ M).

associated with slight red shifting to the fluorescence $\lambda_{max}$ from 340 nm to 344 nm.

These effects indicated interaction processes between HSA and each of safranal and crocin. Binding of HSA to ligand molecules are known to induce conformational changes in the protein secondary structure. The extents of these changes are dependent on the type and strength of the binding force (i.e. electrostatic, hydrophobic, hydrogen bonding … etc.). Ligands' bindings in the close proximity of the tryptophan and tyrosine fluorescent residues quench the fluorescence emission of HSA [41]. The magnitude of such quenching is dependent on the extent of alterations in the fluorogen's environment, ligand's concentration and stability of formed complexes [54,55].

Thus, quenching of HSA fluorescence emissions upon adding safranal or crocin can be explained on the basis of alterations in the environments of the tryptophan and tyrosine chromophores as well as to alteration in HSA's structural conformation upon the formation of HSA-safranal and HSA-crocin complexes [56]. As tryptophan and tyrosine fluorescent chromophores are located on subdomains IIA and IIIA, it seems that safranal and crocin interact mainly with these subdomains.

Shifting the fluorescence $\lambda_{max}$ to longer wavelength upon interactions of HSA with ligand molecules, has been ascribed to the involvement of polar interactions. Thus, it seems that binding of safranal and crocin to HSA encompasses contributions from hydrophobic and hydrogen bonding which is supported by previous UV–Vis measurements [56].

These findings are similar to findings reported by Gonzalez on chlorphenilamine [57], Zhang on pazufloxacinmesilate [58] and Varlan on 3-Carboxyphenoxathiin [59]. The findings are also valuable for the efforts to improve the actions of safranal and crocin in the treatments of diseases [60].

Further conformations on bindings of HSA with safranal and crocin were obtained using CD and molecular docking in sections 3.4 and 3.5.

### 3.3. Binding constants

In this section, the types of binding forces, the number of binding sites, the binding constants, and the nature of fluorescence quenching involved in the interactions of HSA with safranal and crocin will be evaluated. Models based on Stern-Volmer [55], Hill [40], Benesi-Hildebrand [45] and Scatchard [61], will be applied.

Fig. 6a shows Stern-Volmer plots of HSA fluorescence ($F_o/F$) versus concentrations of safranal or crocin as quenchers (Equation (1)). Linear plots were obtained indicating static quenching processes. The slopes of these plots gave $K_{SV}$ value of $1.40 \times 10^4$ L mol$^{-1}$ for safranal and $1.48 \times 10^4$ L mol$^{-1}$ for crocin (Table 1). Using the reported fluorescence life time of HSA; $\tau_0 = 10^{-8}$ s, quenching constants (Kq) of

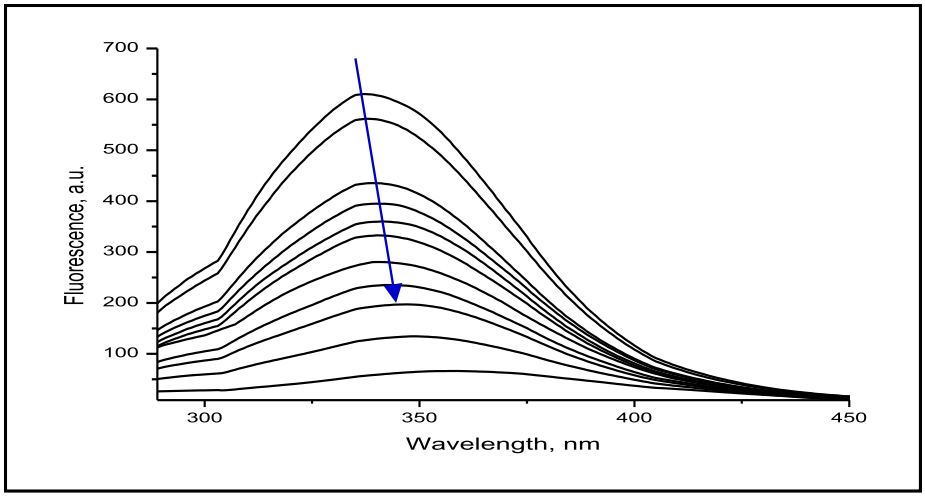


**Fig. 5b.** Fluorescence titration of HSA ($7.5 \times 10^{-6}$ M) with 12 μl increments of safranal ($1 \times 10^{-3}$ M).

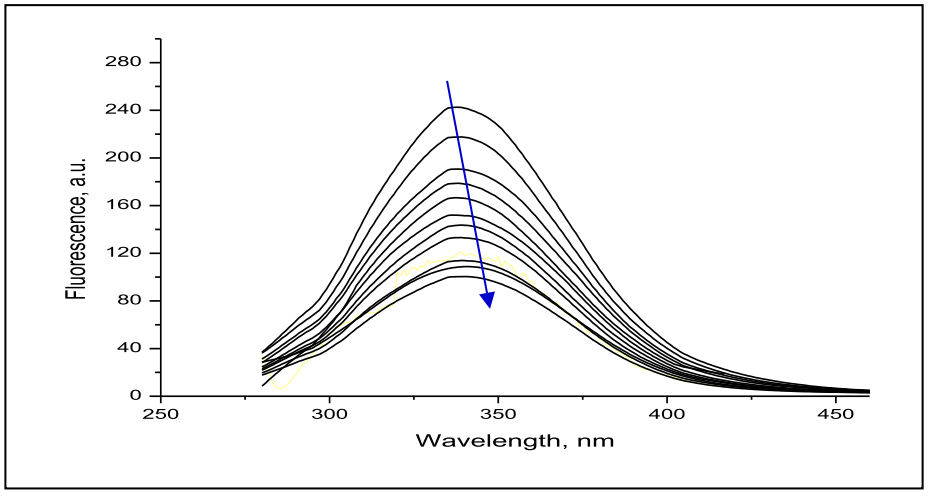


**Fig. 5c.** Fluorescence titration of HSA ($7.5 \times 10^{-6}$ M) with 10 μl increments of crocin ($1 \times 10^{-3}$ M).

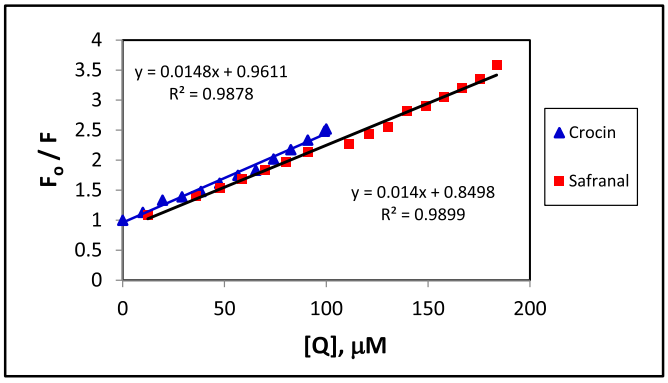


**Fig. 6a.** Stern-Volmer plots of HSA binding with safranal and crocin. The plot represents the fluorescence ratio of HSA ($F_o/F$) versus μM concentrations of safranal or crocin. HSA fluorescence was measured at 340 nm using excitation wavelengths of 278 nm. (Equation (1)).

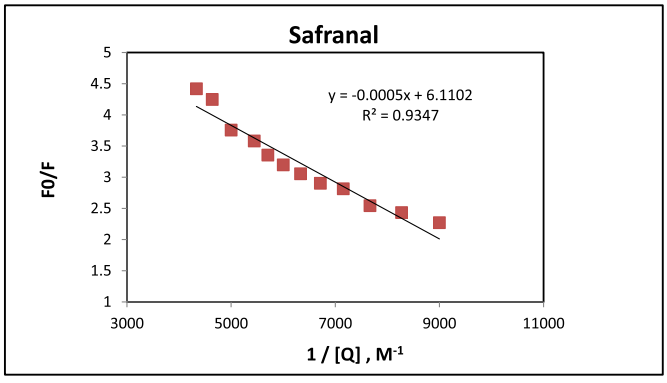


**Fig. 6b.** Stern-Volmer plots of HSA binding with safranal. Fluorescence ratio of HSA ($F_o/F$) versus 1/[Q] M concentration of safranal. HSA fluorescence was measured at 340 nm using excitation wavelengths of 278 nm (Equation (2)).

**Table 1**
Stern Volmer constants (Ksv) and static quenching rate constants (Kq) of safranal and crocin interaction with HSA. R gives the linear correlation coefficients.

| Compound | $K_{SV}$ ($Lmol^{-1}$) | Kq ($Lmol^{-1}s^{-1}$) | R |
|---|---|---|---|
| Safranal | $1.40 \times 10^4$ | $1.40 \times 10^{12}$ | 0.99 |
| Crocin | $1.48 \times 10^4$ | $1.48 \times 10^{12}$ | 0.99 |

$1.40 \times 10^{12}$ L $mol^{-1}.s^{-1}$ for safranal and $1.48 \times 10^{12}$ L $mol^{-1}.s^{-1}$ for crocin were obtained (Table 1) [55]. These quenching constants exceeded the $2.0 \times 10^{10}$ L $mol^{-1}.s^{-1}$ reported controlled diffusion rate constant in aqueous solution [62]. Subsequently our results confirm a static quenching mechanism in which a non-fluorescent ground state complexes of HSA -as a fluorophore- and safranal or crocin -as quenchers-are formed, rather than a dynamic diffusion mechanism involve the collisions of quenchers with the excited fluorophore. The stern Volmer plots of $F_o/F$ versus Log [Q] of safranal or crocin yielded correlation coefficients of 0.99. This has further supported that a static quenching mechanism for HSA fluorescence is dominant in our fluorophore-quencher systems (Table 1).

Binding constants were calculated using Stern-Volmer plots of $F_o/F$ versus reciprocal concentrations of ligands (Equation (2)). Fig. 6b–c shows linear graphs of $F_o/F$ for HSA versus 1/[Q] for added increments of safranal and crocin. Binding constants were obtained by dividing the intercepts with slopes. The binding constants of $1.23 \times 10^4$ and

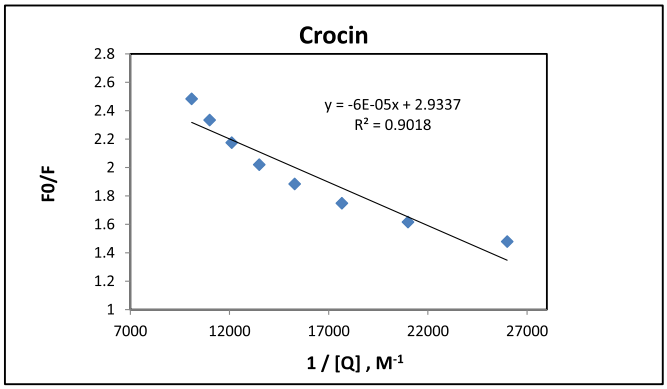


**Fig. 6c.** Stern-Volmer plots of HSA binding with crocin. Fluorescence ratio of HSA ($F_o/F$) versus 1/[Q] M concentration of crocin. HSA fluorescence was measured at 340 nm using excitation wavelengths of 278 nm (Equation (2)).

$4.89 \times 10^4$ L $mol^{-1}$ were respectively obtained for safranal and crocin (Table 2). These values are in good agreements with the binding constants reported for safranal [39], 5-iodouracil, 2-mercapto-1-methylimidazole and 6n-propyl-2-thiouracil [40].

Applications of Hill model for the changes in fluorescence intensity of HSA at 340 nm upon addition of safranal or crocin increments are shown in Fig. 6d. Hill linear plots of log $(F_o - F)/F$ versus log [Q] were obtained. These plots revealed binding constants of $7.67 \times 10^3$ and $3.25 \times 10^3$ L $mol^{-1}$ for safranal and crocin, respectively. The plots also

**Table 2**
Binding constants and binding sites of safranal and crocin interactions with HSA using Stern-Volmer, Hill, Benesi Hildbrand and Scatchard plots.

| Method | Safranal | | | Crocin | | |
|---|---|---|---|---|---|---|
| | K ($Lmol^{-1}$) | Number of binding sites (n) | R | K ($Lmol^{-1}$) | Number of binding sites (n) | R |
| Stern-Volmer Plot | $1.23 \times 10^4$ | – | 0.85 | $4.89 \times 10^4$ | – | 0.82 |
| Hill Plot | $7.63 \times 10^3$ | 1.28 | 0.99 | $3.25 \times 10^3$ | 1.14 | 0.99 |
| Benesi-Hildbrand Plot | $4.25 \times 10^3$ | – | 1.00 | $5.18 \times 10^3$ | – | 0.99 |
| Scatchard Plot Type 1 Site | $2.15 \times 10^5$ | 22 | 0.95 | $4.23 \times 10^5$ | 10 | 0.96 |
| Scatchard Plot Type 2 Site | $2.92 \times 10^4$ | – | 0.95 | $2.56 \times 10^4$ | – | 0.94 |

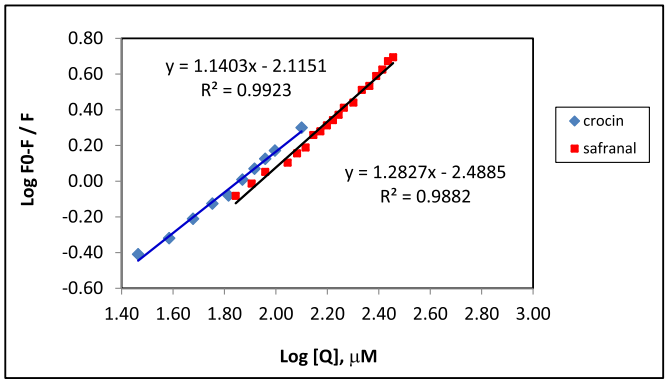


**Fig. 6d.** Hill plots for the binding of safranal and crocin with HSA. Excitation and fluorescence wavelengths are 278 and 340 nm, respectively.

revealed 1.28 and 1.14 binding sites per HSA molecule for safranal and crocin, respectively (Equation (3) and Table 2). These values indicate good affinity for binding HSA to both compounds with 1:1 stoichiometry. Similar values were reported for binding uracil to HSA [40].

Since quenches in fluorescence intensity of HSA is caused by alterations in the microenvironments of the tyrosine and tryptophan (Trip 214) residues in the hydrophobic cavity of subdomains IIA and IIIA, these results confirm that safranal and crocin are preferentially interacting with both domain sites.

On the other hand, the UV–Vis absorptions bands of HSA at 220 and 280 nm have been attributed to the α-helix structure of the protein and the aromatic amino acid residues, respectively [43]. Thus, changes in absorbance of HSA band at 280 nm upon binding with safranal or crocin indicated alterations in the close proximity environment of the amino acid residues [43].

Applications of Benesi-Hildebrand [44] model to changes in the UV–Vis absorption spectra of HSA upon additions of safranal and crocin are shown in Fig. 7a. Benesi-Hildebrand plots of the reciprocals of $(A_{obs} - A_o)$ versus safranal or crocin concentrations gave linear plots with regression coefficients of 0.995 and 0.989, respectively (Equation (6)). Dividing the intercepts with slopes gave the association constants; $4.25 \times 10^3$ and $5.18 \times 10^3$ L $mol^{-1}$ for binding safranal and crocin, respectively. These values are almost similar to the above values obtained by Hill plots.

Scatchard model was also applied to the UV–Vis titration data of safranal and crocin with HSA from Figs. 3a and 4a (Equation (7)). The nonlinear upward-curved Scatchard plots shown in Fig. 7b, were obtained. These plots suggested that safranal and crocin bind to two types of binding sites (1 & 2) on HSA with *negative-negative cooperativity* (i.e. binding on one site decreases the affinity for binding on the other sites) [61]. Graphical analysis of each plot resulted in two intersecting lines.

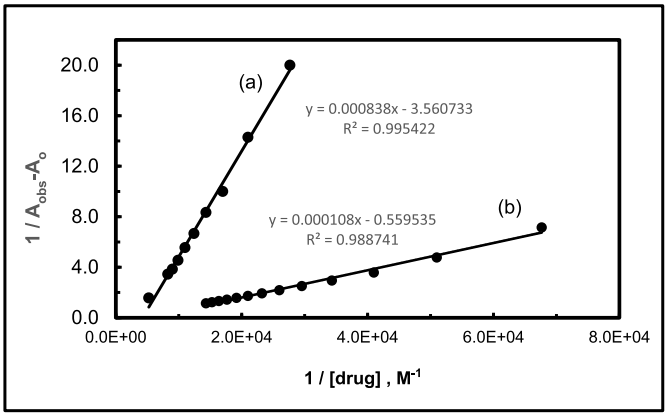


**Fig. 7a.** Benesi Hildbrand plots for the interactions of safranal (a) and crocin (b) with HSA. Plots are based on measuring the absorbance changes at HSA $\lambda_{max}$ of 280 nm.

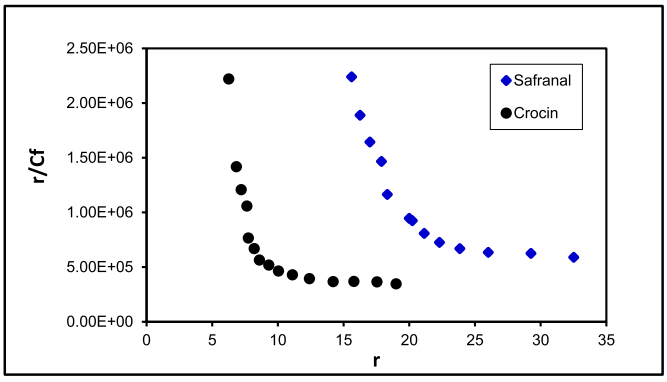


**Fig. 7b.** Nonlinear Scatchard plots for the interactions of safranal (blue line) and crocin (black line) with HSA. Plots are based on measuring the absorbance change at $\lambda_{max}$ of safranal and crocin.

The slope and intercept of each line gave the binding constant and number of binding sites at each type of binding sites (Table 2) [62].

HSA interaction with safranal gave binding constants of $2.15 \times 10^5$ and $2.925 \times 10^4$ L $mol^{-1}$ while crocin gave $4.23 \times 10^5$ and $2.56 \times 10^4$ L $mol^{-1}$ at binding sites types 1 and 2, respectively. Similar values were reported for binding constants of warfarin and diazepam on HSA ($3.4 \times 10^5$ and $3.8 \times 10^5$ L $mol^{-1}$, respectively) [36]. Scatchard plots also revealed 22 binding sites for safranal and ten binding sites for crocin on HSA (Table 2). Binding constants calculated by Scatchard method are 1–2 orders of magnitudes higher than those determined by Stern–Volmer, Hill and Benesi-Hildebrand models. The reason is not fully justified, but it might be correlated with the linearity in plots or sensitivity of different techniques.

The two types of binding sites may encompass specific hydrophobic binding and nonspecific hydrophilic binding (e.g. H-bonding). These results are in accordance with our previous conclusion that safranal and crocin bind on subdomains IIA and IIIA. Thus, our results suggest that safranal and crocin binding to HSA involve contributions from hydrophobic and hydrophilic binding forces.

These conclusions are also consistent with the HSA's fluorescence quenching and decreases in its absorbance upon additions of safranal or crocin discussed in previous sections. Fluorescence quenching has been attributed to alteration in the tryptophan residue (Trp-214) deeply buried in the hydrophobic loop of subdomain IIA and to tyrosine residues located in other subdomains IIIA. Decrease in absorbance was attributed to binding on amino acid residues located in subdomain IIIA and others. Thus, the more hydrophobic IIA site seems more susceptible to hydrophobic molecule while the more hydrophilic IIIA site seems

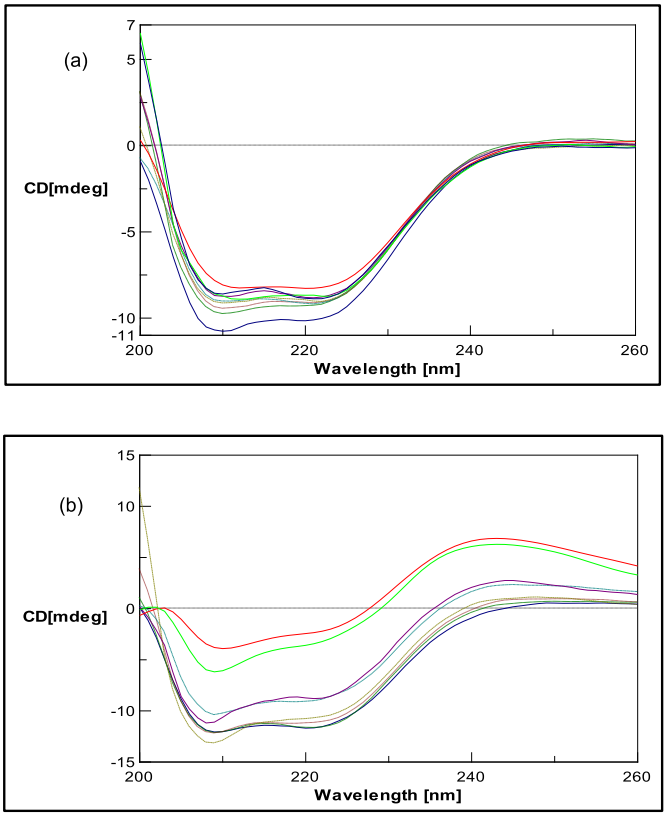


**Fig. 8.** Changes in CD spectra of HSA ($7.5 \times 10^{-6}$ M) upon additions of $1 \times 10^{-3}$ M safranal (a) or crocin (b). Measurements were made using scan speed of 100 nm/min and bandwidth of 1 nm using 1 cm quartz cell.

more susceptible to the polar molecule. Our results suggest that safranal favors hydrophobic binding while crocin favors hydrophilic binding [40].

### 3.4. Circular dichroism

Circular dichroism is the technique of choice to monitor conformational changes and alterations in secondary structures when globular proteins bind small molecules. In this section, changes in HSA's confirmation upon binding to safranal and crocin will be evaluated using CD.

In CD, the α-helix structure of HSA exhibits two negative bands at 209 and 222 nm and one positive band at 190 nm while the β-helix and random coil structures give a negative band at 218 nm and a positive band at 212 nm, respectively [53]. Fig. 8 shows the CD spectral titration of HSA with safranal (Fig. 8a) and crocin (Fig. 8b). The spectra of HSA shows the two negative bands at 209 and 222 characteristics for the α-helix structure. The negative band at 218 nm and the positive one at 212 nm characteristics for the β sheets and random coil structures are absent. These results confirm the predominance of α-helical structure in our HSA protein solution. Additions of safranal or crocin to HSA decreased the intensities of the negative CD signals at 209 and 220 nm indicating interaction processes resulted in the formation of HSA-Safranal or HSA-crocin complexes (Figs. 8a and 8b).

The mean residue ellipticity (MRE) is given by equation (8) where $\theta_{obs}$ is the observed CD in millidegree, n is the number of amino acid residues on HSA (equals 585), l is the cell path length (equals 1.0 cm) and [HSA] is the molar concentration of HSA. The α-helical content of HSA is calculated using equation (9) at 209 nm and equation (10) at 220 nm [53,63].

$$MRE = \frac{\theta_{obs}}{10\ n\ l\ [HSA]} \quad (deg\ cm^2\ dmol^{-1}) \tag{8}$$

$$\%\ \alpha - helix_{209\ nm} = \frac{MRE_{209\ nm} - 4000}{33000 - 4000}\ x\ 100 \tag{9}$$

$$\%\ \alpha - helix_{220\ nm} = \frac{MRE_{220\ nm} - 2340}{30300}\ x\ 100 \tag{10}$$

Applying the two equations to the native free HSA solution gave 71.39% α-helix% at 209 nm and 69.74% α-helix% of at 220 nm.

Fig. 8 show the effect of adding safranal and crocin ligands to HSA up to a molar ratio of 1:13.3 (HSA:ligand). At 209 nm, the α-helix% structure of HSA decreased by the additions of safranal and crocin from 71.39% in free HSA to 55.39% and 55.92%, respectively (Fig. 8a). At 220 nm, decreases in α-helix% structure from 69.74% in free HSA to 62.27% and 48.54% were respectively obtained (Fig. 8b). These results indicate that safranal unfolded HSA by 16.00% at 209 nm and by 7.47% at 220 nm while crocin unfolded HSA by 15.47% and 21.20% at the two wavelengths, respectively (Fig. 8). Thus, additions of safranal has less significantly changed the shape of HSA CD spectrum indicating the remaining of its structure predominantly α-helical (Fig. 8a), while crocin has more significantly changed the HSA CD spectral shape (21.20%) indicating partial structural transformation from α-helix structure (Fig. 8b).

### 3.5. Molecular docking of safranal and crocin on HSA

In this section, we used molecular docking to evaluate the binding energies, binding modes, binding sites and amino acid residues involved in HSA interactions with safranal and crocin. HSA binding sites to various drugs' molecules have been reported in the Protein Data Bank. Crystal structures of co-crystallized HSA with warfarin (PDB file # 2BXD), diazepam (PDB file # 2BXF), azapropazone (PDB file # 2BX8), ibuprofen (PDB file # 2BXG), indomethacin (PDB file # 2BXK), iodipamide (PDB file # 2BXN) and myristate (PDB files # 2BXQ and 2BXP) were downloaded and their binding sites were identified (Table 3). Using Glide software, we docked safranal and crocin onto the above eight binding sites of HSA. Reliable docking scores were obtained by incorporating flexibility in the ligands and the receptor as per the docking parameters described in section 2.

Safranal gave exothermic binding poses in the eight identified pockets with Glide XP scores ranged between −3.969 and −6.913 kcal/mol. The best scoring was for the myristate binding site; −6.9 kcal/mol (Table 3). Fig. 9 depicts the binding of safranal on different sites of HSA. Safranal seems to bind preferentially on subdomain IIIB (position G, myeistrate-1), followed by subdomain IA (position H, myristrate-2) and then subdomain IIA (positions D-ibuprofen, E-indomethacin and A-warfarin). It apparently binds less preferentially to subdomains IIIA (position B-diazepam) and IB (position C-azapropazone), subsequently. Inspection of amino acid residues involved in each pocket, indicated that binding preference seems to decrease from the more hydrophobic cavity (myristate-1, −6.913 kcal/mol) to the less hydrophobic cavity (iodipamide, −3.969 kcal/mol) [37]. Thus, safranal seems to bind specifically and non-specifically through multiple Van der Waals contacts with the surrounding amino acid residues (Table 3; Fig. 10).

These findings confirm that safranal binds to different sites on HSA which is in high agreement and confirmation with our spectroscopic measurements presented in the previous sections. But, these findings are significantly contradicting with the findings reported by Ali et al. who reported only one principal binding site (sudlow 1) on subdomain IIA-with binding energy −4.55 kcal/mol [38].

On the other hand, molecular docking of crocin onto the above eight active sites gave endothermic Glide scores (Table 3). These results indicated unfavorable binding for crocin onto the eight investigated binding sites. The reason was attributed to the large size and polar

**Table 3**
Glide docking scores, matched PDB codes and site drugs' binding names, binding site label and amino acid residues involved in binding. Results obtained by docking safranal and crocin into human serum albumin.

| Serial | Glide XP Score (kCal/mol) | | Matched PDB code and bonded drug | Binding site label | Protein subdomain | Amino acid residues involved in binding |
|---|---|---|---|---|---|---|
| | Safranal | Crocin | | | | |
| 1 | −4.956 | – | 2BXD Warfarin | A | IIA | Tyr150, Arg257, Ala261, Leu260, Ser287, Leu238, Ile264, His242, Ile290, Arg222 |
| 2 | −4.711 | – | 2BXF Diazepam | B | IIIA | Tyr411, Arg485, Ser489, Asn391, Val433, Leu453, Leu407, Arg110, Lys414, Leu387, Ile388, Leu430, Phe403 |
| 3 | −4.238 | – | 2BX8 Azapropazone | C | IB | Tyr161, Tyr138, Leu182, Arg117, Met123, Glu141, Ile142, Leu115, Glu141 |
| 4 | −6.135 | – | 2BXG, Ibuprofen | D | Sudlow I | Trp214, Val482, Ala210, Leu347, Val343, Val344, Leu481, Ser202, Ser454, Phe211, Leu198 |
| 5 | −5.841 | – | 2BXK Indomethacin | E | Sudlow I | Trp214, Lys199, Leu198, Phe211, Ser202, Ala201, Ala215, Ala210, Leu481, Lys212, Gly207, Phe206, Leu203 |
| 6 | −3.969 | – | 2BXN Iodipamide | F | Sudlow II | Lys436, Asp429, Tyr452, Val455, Val433, Ala191, Ala194, Gln459, Asn429, Lys190, Val456, Leu430, Lys432 |
| 7 | −6.913 | – | 2BXQ Myristate-1 | G | IIIB | Leu14, Leu22, Phe19, Phe70, Ala26, Val23, Leu66, Val46, Val7, Arg10, Leu250, Leu251 |
| 8 | −6.597 | – | 2BXP Myristate-2 | H | IA | Lys525, Ala528, Val547, Leu532, Phe509, Phe551, Phe551, Leu575, Met548, Leu529, Leu544, Phe509, Phe507 |
| 9 | – | −12.922 | Crocin New Binding Site | I | Sudlow I | Trp214, Tyr150, Tyr452, Arg222, Arg218, Glu292, Ala291, Pro447, Lys436, Lys195, Lys199, Val293, Glu294, Ile290, Ser287, Arg218, Glu292, Leu260, Ala261, Arg257, Ser192, His242, Leu238, Glu153, His288, Phe157, Glu188, Ile264, His440, Ala191, Gln196, Lys195, Lys436, Cys448, Asp451, Leu219 |

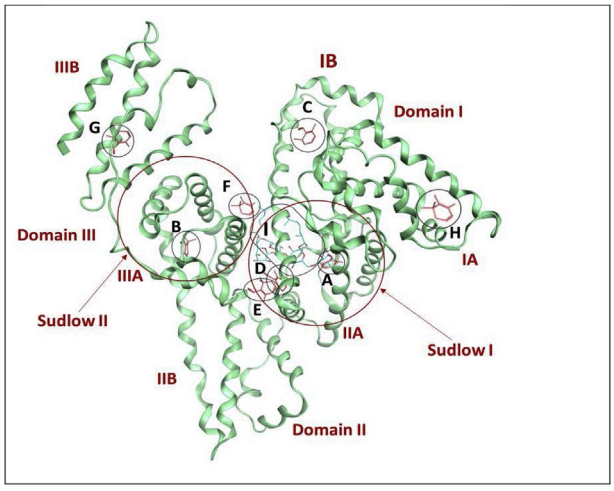


**Fig. 9.** Human serum albumin (HSA) domains, subdomains, sudlow's binding sites I and II (red) and docking sites (**A-I)** of safranal (in pink sticks) and crocin (in blue sticks). (For interpretation of the references to color in this figure legend, the reader is referred to the Web version of this article.)

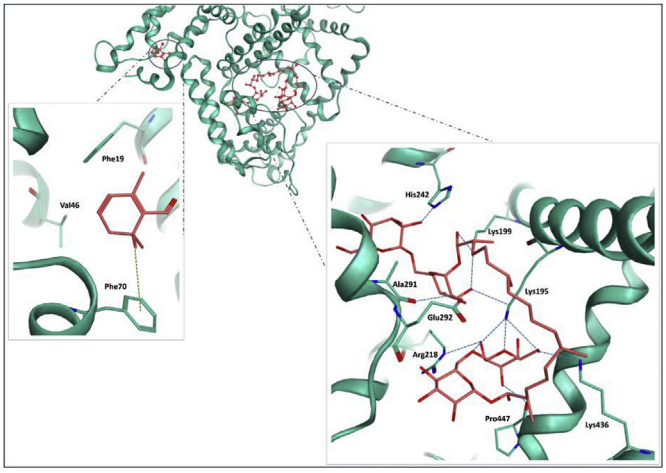


**Fig. 10.** Structure of albumin along with the zoom-in pictures for the binding mode of safranal (left) and crocin (right).

characters of the crocin molecule. Therefore, we scanned HSA molecule for all possible binding sites using by nonspecific blind docking of crocin molecule onto the whole albumin protein domains. The results revealed the finding of a new large exothermic binding pocket/site scored as low as −12.9 kcal/mol. This pocket is located in the sudlow 1 binding site of the subdomain IIA. This site is surrounded with large number of polar amino acid residues that render it hydrophilic character. Crocin can accommodate itself in this large site through multiple hydrogen bonding interactions with surrounding amino acid residues listed in Table 3. This site is a new finding in this work that was not reported before in literature.

Thus our molecular docking suggested that safranal and crocin bind to human serum albumin on two types of binding sites. Safranal preferably binds on the hydrophobic sites of IIIA subdomain. Its next preference binding sites is located in the subdomain IIA. The inside wall of the IIA pocket comprises hydrophobic side chains whereas its entrance is surrounded by positively charged amino acids residues such as RG218, LYS195 and Trip 214. Therefore, this site can bind polar and nonpolar molecules that include crocin. Analysis of binding forces indicated that safranal and crocin are favorably binding to the amino acid residues at each binding site by van der Waals interactions (Table 3) [64,65].

These in-silico molecular docking results suggested spontaneous exothermic reactions involve both hydrophobic and hydrogen bonding interactions between HSA and each of safranal and crocin [37,39]. They are consistent with our spectroscopic measurements and provided structural evidence for quenching HSA's fluorescence by safranal and crocin. They also showed that the forces bind HSA to both compounds are strong enough to control their delivery to target tissues. However, safranal's binding seemed more hydrophobic while crocin's binding seemed more hydrogen bonding.

## 4. Conclusion

Human serum albumin is the most abundant plasma protein in human blood. It solubilizes and transports drugs and other substances

to target tissues in the body. Safranal and crocin are two major phytochemical ingredients from saffron; the herb long used in traditional medicine. They are biologically active with anticancer, antispasmodic, antidepressant and aphrodisiac pharmacological effects.

In this work, we studied the interactions of HSA with safranal and crocin using UV–Vis molecular absorption, fluorescence quenching and circular dichroism spectroscopies as well as molecular docking techniques. Structural changes, binding affinities, binding sites, binding energies, binding forces and amino acid residues involved in bindings were evaluated to gain insights upon the interactions of HSA with safranal and crocin.

Additions of safranal and crocin to HSA decreased its absorbance intensity (at $\lambda_{max}$ = 278 nm). The reason was attributed to binding of the two compounds to amino acid residues chromophores located in subdomains IIA and IIIA of HSA. Additions of safranal and crocin was also found to quench the fluorescence emission of HSA at $\lambda_{max}$ = 340 nm. This effect was correlated with binding to tyrosine and tryptophan amino acids fluorogen and structural changes in the micro environment of these chromophores upon interactions. In our measurements, the inner filter effects were excluded using $\lambda_{excit}$ of 278 nm and $\lambda_{fluores.}$ of 340 nm for HSA while safranal and crocin absorbed maximally at 320 and 445 nm, respectively.

Application of Stern-Volmer model to fluorescence quenching measurements revealed quenching constants (Kq) of $1.40 \times 10^{12}$ and $1.48 \times 10^{12}$ L mol$^{-1}$.s$^{-1}$ for safranal and crocin, respectively. These values indicated a static quenching mechanism involve the formation of non-fluorescent ground state HSA complexes. Applications of Stern-Volmer, Hill, Benesi-Hilbrand and Scatchard models revealed apparent binding constants ranged in $4.25 \times 10^{3}$ - $2.15 \times 10^{5}$ for safranal and $7.67 \times 10^{3}$ - $4.23 \times 10^{5}$ L mol$^{-1}$ for crocin with HSA.

Circular dichroism measurements revealed the unfolding of HSA's α-helix structure by 7.47–21.20% upon addition of 13 folds of safranal or crocin. These results provided additional evidences about changes in HSA conformational structure upon interactions with both compounds.

In-silico molecular docking of HSA using Glide tool revealed selective exothermic binding of safranal on the eight investigated binding sites with binding energies ranged between −3.969 and −6.6.913 kcal/mol. Safranal seemed to preferentially bind on subdomain IIIB, followed by subdomain IA and then subdomain IIA. Crocin was found to exothermally bind on a new large pocket located on subdomain IIA (sudlow 1) with binding energy of −12.922 kcal/mol.

Binding of both compounds involved hydrophobic and hydrophilic interactions with amino acid residues through van der Waals intermolecular forces at each binding site. Safranal binding seemed more hydrophobic while crocin binding seemed more hydrophilic. The reason could be attributed to the difference in their polarities.

These results provided that HSA can solubilize and transport safranal and crocin in blood to target tissues. The results are also of high importance in determining the pharmacological properties of both compounds and for their future developments as therapeutic agents.

## Authors' contribution statement

Dr. A. Salem has contributed to the conceptual idea of the work, designed the experimental study and run the experiments and molecular docking. He also took the responsibility of discussing the results, writing the final versions of the paper and communicating with publishers.

Dr. M. Lotfy participated in running the experiments, plotting results and drafted an initial version of the manuscript.

Dr. A. Amin contributed to the general idea of the work and provided the HSA and saffron compounds used in the study.

Dr. M. Ghattas contributed by running the molecular docking calculation.

## Acknowledgment

The authors gratefully acknowledge the financial support provided by the research affairs at the United Arab Emirates University through the UPAR grant # 31S116. They also acknowledge the students Alaa Al-Hrout and Zuhour Al-Housani for their helps in running the UV–Vis absorption measurements.

## References

[1] B. Javadi, A. Sahebkar, A.A. Emami, A survey on saffron in major islamic traditional medicine books, Iran J. Basic Med. Sci. 16 (2013) 1–11.
[2] H. Hosseinzadeh, M. Nassiri-Asl, Phytother, Ibn Sina's (Ibn sina) the canon of medicine and saffron (crocus sativus): a review, Resume 27 (4) (2013) 475–483.
[3] F. Abdullaev, J. Espinosa-Aguirre, Biomedical properties of saffron and its potential use in cancer therapy and chemoprevention trials, Cancer Detect, Prevue 28 (2004) 426–432.
[4] I. Das, S. Das, T. Saha, Saffron suppresses oxidative stress in DMBA induced skin carcinoma: a histopathological study, Acta Histochem. 112 (4) (2010) 317–327.
[5] J. Rios, M. Recio, R. Giner, S. Manez, An update review of saffron and its active constituents, Phytother Res. 10 (3) (1996) 189–193.
[6] F.I. Abdullaev, N.L. Riverón, O.H. Caballero, H.J. Manuel, L.I. Pérez, M.R. Pereda, A.J. Espinosa, Use of in vitro assays to assess the potential antigenototoxic and cytotoxic effect of saffron (Crocus sativus), Toxicol. In *Vitro* 17 (2003) 731–736.
[7] A.N. Assimopoulou, Z. Sinakos, V.P. Papageorgiou, Radical scavenging activity of *Crocus sativus* L. extract and its bioactive constituents, Phytother Res. 19 (2005) 997–1000.
[8] H. Hosseinzadeh, F. Shamsaie, S. Mehri, Antioxidant activity of aqueous and Ethanolic extracts of *Crocus sativus* L. stigma and its bioactive constituents crocin and safranal, Pharmacogn. Mag. 5 (2010) 419–424.
[9] H. Hosseinzadeh, H.R. Sadeghnia, Effect of safranal, a constituent of *Crocus sativus* (saffron), on methyl methanesulfonate (MMS)-induced DNA damage in mouse organs: an alkaline single-cell gel electrophoresis (comet) assay, DNA Cell Biol. 26 (2007) 841–846.
[10] M.H. Boskabady, M.R. Aslani, Relaxant effect of Crocus sativus (saffron) on Guinea-pig tracheal chains and its possible mechanisms, J. Pharm. Pharmacol. 58 (2006) 385-1390.
[11] J. Behravan, H. Hosseinzadeh, A. Rastgoo, O.M. Malekshah, M. Hessani, Evaluation of the cytotoxic activity of crocin and safranal using potato disc and brine shrimp assays, Physiol. Pharmacol. 13 (2010) 397–403.
[12] H. Hosseinzadeh, J. Ghenaati, Evaluation of the antitussive effect of stigma and petals of saffron (Crocus sativus) and its components, safranal and crocin in Guinea pigs, Fitoterapia 77 (2006) 446–448.
[13] H. Hosseinzadeh, H.R. Sadeghnia, Protective effect of safranal on pentylenetetrazol-induced seizures in the rat: involvement of GABAergic and opioids systems, Phytomedicine 14 (4) (2007) 256–262.
[14] H. Hosseinzadeh, V.M. Shariaty, Anti-nociceptive effect of safranal, a constituent of Crocus sativus (saffron), in mice, Pharmacologyonline 2 (2007) 498–503.
[15] B. Amin, H. Hosseinzadeh, Evaluation of aqueous and ethanolic extracts of saffron, *Crocus sativus* L., and its constituents, safranal and crocin in allodynia and hyperalgesia induced by chronic constriction injury model of neuropathic pain in rats, Fitoterapia 83 (2012) 888–895.
[16] H.R. Sadeghnia, M.A. Cortez, D. Liu, H. Hosseinzadeh, S.O. Carter, Protective effect of Crocus sativus stigma extract and crocin (trans-crocin 4) on methyl methanesulfonate-induced DNA damage in mice organs, J. Pharm. Pharm. Sci. 11 (2008) 1–14.
[17] H. Hosseinzadeh, G. Karimi, M. Niapoor, Antidepressant effects of Crocus sativus stigma extracts and its constituents, crocin and safranal, in mice, Acta Hortic. (Wagening.) 650 (2004) 435–445.
[18] M. Imenshahidi, H. Hosseinzadeh, Y. Javadpour, Hypotensive effect of aqueous saffron extract (Crocus sativus L.) and its constituents, safranal and crocin, in normotensive and hypertensive rats, Phytother Res. 24 (2010) 990–994.
[19] H. Hosseinzadeh, N.B. Noraei, Anxiolytic and hypnotic effect of Crocus sativus aqueous extract and its constituents, crocin and safranal, in mice, Phytother Res. 23 (2009) 768–774.
[20] H. Hosseinzadeh, S. Mehri, M.M. Abolhassani, M. Ramezani, A. Sahebkar, K. Abnous, Affinity-based target deconvolution of safranal, DARU J. Pharm. Sci. 21 (1) (2013) 25.
[21] C.D. Kanakis, P.A. Tarantilis, H.A. Tajmir-Riahi, M.G. Polissiou, Inhibitory activity on amyloid-beta aggregation and antioxidant properties of Crocus sativus stigmas extract and its crocin constituents, J. Agric. Food Chem. 55 (2007) 970–977.
[22] M. Papandreou, C. Kanakis, M. Polissiou, S. Efthimiopoulos, P. Cordopatis, M. Margarity, F. Lamari, Inhibitory activity on amyloid-beta aggregation and antioxidant properties of Crocus sativus stigmas extract and its crocin constituents, J. Agric. Food Chem. 54 (23) (2006) 8762–8768.
[23] S. Saleem, M. Ahmad, A.S. Ahmad, S. Yousuf, M.A. Ansari, M.B. Khan, T. Ishrat, F. Islam, Effect of Saffron (*Crocus sativus*) on neurobehavioral and neurochemical changes in cerebral ischemia in rats, J. Med. Food 9 (2) (2006) 246–253.
[24] F.I. Abdullaev, Inhibitory effect of crocetin on intracellular nucleic acid and protein synthesis in malignant cells, Toxicol. Lett. 70 (1994) 243–251.
[25] P.A. Tarantilis, H. Morjani, M. Polissiou, M. Manfait, Inhibition of growth and induction of differentiation of promyelocytic leukaemia (HL-60) by carotenoids from *Crocus sativus*, Anticancer Res. 14 (5A) (1994) 1913–1918.

[26] S.C. Nair, S.K. Kurumboor, J.H. Hasegawa, Saffron chemoprevention in biology and medicine, A review, Cancer Biother. 10 (4) (1995) 257–264.
[27] M. Ashrafi, S.Z. Bathaie, M. Taghikhani, A.A. Moosavi-Movahedi, The effect of carotenoids obtained from saffron on histone H1 structure and H1–DNA interaction, Int. J. Biol. Macromol. 36 (4) (2005) 246–252.
[28] C.D. Kanakis, P.A. Tarantilis, C. Pappas, J. Bariyanga, H.A. Tajmir-Riahi, M.G. Polissiou, An overview of structural features of DNA and RNA complexes with saffron compounds: models and antioxidant activity, J. Photochem. Photobiol. B Biol. 95 (3) (2009) 204–212.
[29] A.M. Merlot, D.S. Kalinowski, D.R. Richardson, Unraveling the mysteries of serum albumin -more than just a serum protein, Front. Physiol. 5 (2014) 299.
[30] M. Fasano, S. Curry, E. Terreno, M. Galliano, G. Fanali, P. Narciso, S. Notari, P. Ascenzi, The extraordinary ligand binding properties of human serum albumin, IUBMB Life 57 (12) (2005) 787–796.
[31] F. Tan, M. Guo, Q. Yu, Studies on interaction between gatifloxacin and human serum albumin as well as effect of copper (II) on the reaction, Spectrochim. Acta A Mol. Biomol. Spectrosc. 61 (13) (2005) 3006–3012.
[32] H. Gao, L. Lei, J. Liu, Q. Kong, X. Chena, Z. Hua, The study on the interaction between human serum albumin and a new reagent with antitumour activity by spectrophotometric methods, J. Photochem. Photobiol., A 167 (2004) 213–221.
[33] W.Y. Choi, S. Kim, N. Lee, M. Kwon, I. Yang, M. Kim, S.G. Cheong, D. Kwon, J.Y. Lee, H.B. Oh, C. Kang, Amantadine-resistant influenza A viruses isolated in South Korea from 2003 to 2009, Antivir. Res. 84 (2) (2009) 199–202.
[34] W. Ang, E. Daldini, L. Juillerat-Jeanneret, P. Strategy, Strategy to tether organometallic ruthenium − arene anticancer compounds to recombinant human serum albumin, Inorg. Chem. 46 (22) (2007) 9048–9050.
[35] A.R. Timerbaev, C.G. Hartinger, S.S. Aleksenko, B.K. Keppler, Interactions of antitumor metallodrugs with serum proteins: advances in characterization using modern analytical methodology, Chem. Rev. 106 (6) (2006) 2224–2248.
[36] U.K. Hansen, V.T.G. Chuang, M. Otagiri, Practical aspects of the ligand-binding and enzymatic properties of human serum albumin, Biol. Pharm. Bull. 25 (6) (2002) 695–704.
[37] J. Ghuman, P.A. Zunszain, I. Petitpas, A.A. Bhattacharya, M. Otagiri, S. Curry, Structural basis of the drug binding specificity of human serum albumin, J. Mol. Biol. 353 (2005) 38–52.
[38] P.B. Kandagal, S.S. Kalanur, D.H. Manjunatha, J. Seetharamappa, Mechanism of interaction between human serum albumin and N-alkyl phenothiazines studied using spectroscopic methods, J. Pharm. Biomed. Anal. 47 (2) (2008) 260–267.
[39] M.S. Ali, H.A. Al-Lohedan, Spectroscopic and computational evaluation on the binding of safranal with human serum albumin: role of inner filter effect in fluorescence spectral correction, Spectrochim. Acta A Mol. Biomol. Spectrosc. 203 (2018) 434–442.
[40] A. Sułkowska, Interaction of drugs with bovine and human serum albumin, J. Mol. Struct. 614 (2002) 227–232.
[41] D.C. Carter, J.X. Ho, Structure of serum albumin, Adv. Protein Chem. 45 (1994) 153–203.
[42] R. Swarup, Review on Interaction of serum albumin with drug molecules, J. Pharm. Toxicol. Studies (RRJPTS) 4 (2) (2016) 7–16.
[43] F. Samari, B. Hemmateenejad, M. Shamsipur, M. Rashidi, H. Samouei, Affinity of two novel five-coordinated anticancer Pt(II) complexes to human and bovine serum albumins: a spectroscopic approach, Inorg. Chem. 51 (2012) 3454–3464.
[44] H.A. Benesi, J.H. Hildebrand, A Spectrophotometric investigation of the interaction of iodine with aromatic hydrocarbons, J. Am. Chem. Soc. 71 (1949) 2703.
[45] T. Hiratsuka, Conformational changes in the 23-kilodalton NH2-terminal peptide segment of myosin ATPase associated with ATP hydrolysis, J. Biol. Chem. 265 (31) (1990) 18786–18790.
[46] Molecular operating environment, Chemical computing group (Montreal, Canada), http://www.chemcomp.com.
[47] M. Brisson, T. Nguyen, A. Vogt, J. Yalowich, A. Giorgianni, D. Tobi, I. Bahar, C.R.J. Stephenson, P. Wipf, J.S. Lazo, Discovery and characterization of novel small molecule inhibitors of human Cdc25B dual specificity phosphatase, Mol. Pharmacol. 66 (4) (2004) 824–833.
[48] Small-Molecule Drug Discovery Suite 2015-2: Glide, Schrödinger, LLC, New York, NY, 2015 version 6.7.
[49] W.L. Jorgensen, J. Tirado-Rives, The OPLS [optimized potentials for liquid simulations] potential functions for proteins, energy minimizations for crystals of cyclic peptides and crambin, J. Am. Chem. Soc. 110 (6) (1988) 1657–1666.
[50] R.A. Friesner, R.B. Murphy, M.P. Repasky, L.L. Frye, J.R. Greenwood, T.A. Halgren, P.C. Sanschagrin, D.T. Mainz, Extra precision glide: docking and scoring incorporating a model of hydrophobic enclosure for protein − ligand complexes, J. Med. Chem. 49 (21) (2006) 6177–6196.
[51] P.A. Tarantilis, G. Tsoupras, M. Polissiou, Determination of saffron (Crocus sativus L.) componenets in crude plant extract using high performance liquid chromatography –UV-Vis photodiode-array detection–mass spectrometry, J. Chromatogr. A 669 (1995) 107–118.
[52] S.M. Khan, D.W. Darnell, E.R. Birnbaum, Biochim. Biophys. Tyrosine fluorescence as a measure of denaturation in thermolysin, Acta 624 (1980) 1–12.
[53] J.R. Lakowicz, Principles of Fluorescence Spectroscopy, third ed., Springer US, 2006.
[54] M. Kumari, J.K. Maurya, M. Tasleem, P. Singh, R. Patel, Probing HSA-ionic liquid interactions by spectroscopic and molecular docking methods, J. Photochem. Photobiol. B Biol. 138 (2014) 27–35.
[55] J. Li, Y. Jiao, C. Dong, Spectroscopic analysis and molecular modeling on the interaction of jatrorrhizine with human serum albumin (HSA), Spectrochim. Acta A Mol. Biomol. Spectrosc. 24 (118) (2014) 48–54.
[56] S. Rubio, A. Gomez-Hens, M. Valcarcel, Analytical applications of synchronous fluorescence spectroscopy, Talanta 33 (1986) 633–640.
[57] J.J. Gonzalez, Analysis of the binding of chlorpheniramine to human serum albumin by spectroscopic techniques, Chem. Biol. Interact. 91 (1994) 65–74.
[58] J. Jin, X. Zhang, J. Spectrophotometric studies on the interaction between pazufloxacinmesilate and human serum albumin or lysozyme, Luminescence 128 (2008) 81–86.
[59] A. Varlan, M. Hillebrand, Bovine and human serum albumin interactions with 3-carboxyphenoxathiin studied by fluorescence and circular dichroism spectroscopy, Molecules 15 (6) (2010) 3905–3919.
[60] S. Gorinstein, I. Goshev, S. Moncheva, M. Zemser, M. Weisz, A. Caspi, I. Libman, H.T. Lerner, S. Trakhtenberg, O.M. Belloso, Intrinsic tryptophan fluorescence of human serum proteins and related conformational changes, J. Protein Chem. 19 (8) (2000) 637–642.
[61] A.K. Bordbar, A.A. Saboury, A.A. Moosavi-Movahedi, The shapes of Scatchard plots for systems with two sets of binding sites, Biochem. Educ. 24 (3) (1996) 172–175.
[62] N.J. Greenfield, G.D. Fasman, Computed circular dichroism spectra for the evaluation of protein conformation, Biochemistry 8 (10) (1969) 4108–4116.
[63] J. Matei, S. Ionescu, M. Hillebrand, Interaction of fisetin with human serum albumin by fluorescence, circular dichroism spectroscopy and DFT calculations: binding parameters and conformational changes, J. Lumin. 131 (2011) 1629–1635.
[64] B. Meloun, L. Moravek, V. Kostka, Complete amino acid sequence of human serum albumin, FEBS (Fed. Eur. Biochem. Soc.) Lett. 58 (1–2) (1975) 134–137.
[65] M. Dockal, D.C. Carter, F. Ruker, The three recombinant domains of human serum albumin. Structural characterization and ligand binding properties, J. Biol. Chem. 274 (41) (1999) 29303–29310.